MANSOURA JOURNAL OF PHYSICS
Official Journal of Faculty of Science, Mansoura University, Egypt
E-mail: scimag@mans.edu.eg ISSN: 2974-4954

Preparation and Characterization of Nickel Chlorapatite Composite

Marwa E. Sobh*, G. El-Damrawi, H. Doweidar, K El-Egili

Glass Research Group, Physics Department, Faculty of Science, Mansoura University, 35516, Egypt

**Corresponding author: marwaelsaid666@gmail.com*

Received:16/6/2021
Accepted:21/8/2021

Abstract: A series of Ni-substituted chlorapatite, $(Ni_xCa_{1-x})_5(PO_4)_3Cl$, where x= 0, 5, 10, 15 and 20, was prepared by a solution gelation method. The calcium nitrate was used as a calcium source and di ammonium hydrogen phosphate as preferred source for P_2O_5 phosphorus. The Ca:P and Ca:Cl molar ratios were fixed near the specific known values, 1.67 and 5 respectively. As prepared samples were subjected to specific sintering processes at various temperatures, particularly at 700°C, 800°C, and 900°C. X-ray diffraction (XRD), Scanning electron microscopy (SEM), Energy-dispersive X-ray spectroscopy (EDX), and Fourier transform infrared spectroscopy (FT-IR) were used to evaluate the prepared sample of various compositions. The XRD and FTIR spectra have confirmed that the chlorine ions can be incorporated in the apatite structure. The absorption bands associated to the Cl, OH^-, (PO_4^{3-}) functional groups that characterize the chlorapatite (CLAP) and hydroxyapatite (HAP) phases are highly defined and resolved in the FTIR spectra. Both chlorapatite $Ca_5(PO_4)_3Cl$ and calcium nickel phosphate (Ni doped chlorapatite) phases are simply identified. The analysis suggest that the Ni doped CLAP calcined at 800 ^oC for 1 hour is the main formed crystalline phase. Incorporation of Ni atoms into chlorapatite phase well result in increasing porosity of the whole prepared material. The SEM observations lead to suggest that, the obtained CLAP phases are constructed mainly in the form of crystalline-grains morphology.

Keywords: Apatite, Nickel chlorapatite, X-ray diffraction, SEM

1.Introduction

Apatite is a group of phosphate minerals, usually referring to calcium phosphate crystals $Ca_3(PO_4)_2$, When this crystal interacts with OH groups, the Hydroxyapatite mineral phase (HA) is the main product. Although the AH structure is known with its highest bioactivity, but its mechanical strength is very week [1, 2]. Therefore, additional molecules or atoms such as F, Ni, Cl, Ce, etc…, should be added to the chemical patches to enhance the strength of the well-prepared HA [3]. In such situation, Fluor apatite and chlorapatite, with high concentrations of OH^-, F^- and Cl^- ions are the most recommended to be prepared and used. Phosphate-bearing apatite is generally characterized by the formula $M_{10}(PO_4)_6X_2$ (M and X represent cations and anions, respectively) [4]. One of the features of apatite is the ability to exchange cations and anions in the structure. As a kind of apatite, chlorapatite $[Ca_{10}(PO_4)_6Cl_2$ (CLAP)] is an ideal material for heavy metal removal since the complexes of CLAP and heavy metal were highly stable under oxidizing and reducing conditions, and CLAP has a high adsorption capacity for heavy metals [5-8].

The presence of some chlorine ions in the HA crystal lattice can improve its resorption as well as mechanical properties. Chlorapatite can be easily synthesized and has no toxicity to organism [9, 10]. Due to its variable pore size, CLAP is a suitable porous material for loading other Nano sized structures, e.g., metals and dyes [11]. It can also transfer the metals from unstable to stable fraction and reduces the toxicity by precipitation, ion exchange and adsorption effect [12-15]. In addition, chlorapatite is poorly soluble in the water and non-soluble in alkaline solutions, but easily dissolve in acids

[16]. There is additional Nickel is good alternative material because its more economical than gold and silver and it has antibacterial activity [17, 18]. Many materials such as silver, iron and nickel were tested and proved their ability to improve the CLAP properties. Usually Ca atoms are substituted by metal atom via the method of solution gelation process [19]. The metal can regularly have distributed in the composite structure providing stable metal chlorapatite (metal inside matrix) as an example calcium nickel phosphate ($Ca_{19}Ni_2$ $(PO_4)_{14}$) with JCPDS file no. [49-122].

The present work aimed to synthesize pure chlorapatite and chlorapatite doped with different concentration of nickel chloride by solution method to achieve two objectives. One of them is to prepare chlorapatite and calcium nickel phosphate to study the phase stability and powder characteristics. The latter are used in treatment of wastewater application.

2. Materials and Procedures

2.1 Chlorapatite synthesis:

Calcium nitrate tetra hydrate solution and Di-ammonium hydrogen phosphate solution with ammonium chloride were prepared by dissolving the desired amounts in Ethyl alcohol at room temperature on magnetic stirrer for 15 minutes. Calcium nitrate tetra hydrate solution was added to Di-ammonium hydrogen phosphate solution drop wise under continuous stirring for 30 minutes then added drop wise of ammonium hydroxide to adjust pH at 9. Slow titration and diluted solutions were used to improve chemical homogeneity and stoichiometry within the system. The resulting solution was aged for 3 days. After aging, the precipitates obtained were evaporated in air. The resulting gel was oven-dried at 100 °C for 1 hour then calcite at 700°C, 800°C and 900°C for 1h. Figure (1) represents flowchart used for preparation of chlorapatite through chemical route.

2.2 Synthesis of Ni-substituted chlorapatite (CLAP):

The presence of different metal ions in apatite improves the properties of apatite or new properties were introduction. $NiCl_2.6H_2O$ added to Di-ammonium hydrogen phosphate solution as the flowchart in figure 1.

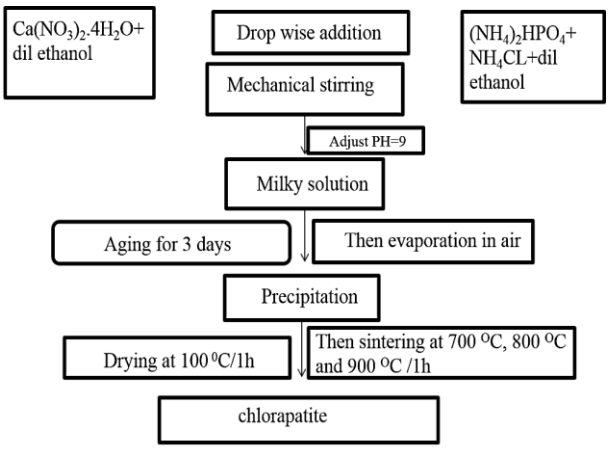

Fig. (1): Flowchart of chlorapatite synthesis.

2.3 Measurement Techniques:

X-Ray diffraction pattern: all the synthesized series samples are characterized by XRD analysis (before and after heat treated at different temperature using a Bruker Axs-D8 Advance diffractometer, equipped with a Cu K_α source (λ=0.15406 nm). 4°-70° is the 2 Θ range of recorded data in step mode, with intervals of 0.02°, using a dwell time of 0.4 seconds. Phase identification was carried out using XPert HighScore Plus. (PANalytical, Netherlands).

2.4 Scanning electron microscope (SEM) with energy dispersive X-ray (EDX) model JEOL-JSM 6510LV, operating at 30 KV, was used to examine the morphology of surface in the prepared samples before and after sintering at different temperature (700, 800 and 900 °C) for 1 hour.

FT-IR absorption spectra of the doped sample sintering were recorded at room temperature using the KBr disk technique. The samples were grinded to fine powder and mixed with KBr at a ratio of 1:100 in weight in an agate mortar. A Mattson 5000 FTIR spectrometer reveals the functional groups which are recorded in the wavenumber range between 4000- 400 cm^{-1} region with a resolution of 2 cm^{-1}. The spectrum of each sample is the average of 30 scans.

3. Results and Discussion

3.1 X-Ray Diffraction

XRD pattern of as prepared chlorapatite and of sintering sample at 700 °C, 800 °C and 900 °C shown in Figure (2). There are several sharp diffraction lines representing specific crystalline phase in the main matrix. The structure of the well-formed crystal is assigned to chlorap-

atite of a hexagonal like structure which is represented by the chemical formula $Ca_{9.97}(PO_4)_6Cl_{1.94}$ [JCPDS card No, 88-2170]. However, it can be observed both the sharpness and intensities of the spectral lines are higher in the case of sample at 800 °C than at other temperatures. This leads that calcination at 800 °C is the more effective in enhancing the crystalline structure of the chlorapatite phase.

There was a secondary phase β tri calcium phosphate [JCPDS card No 06-0426] at 2Θ= 25.9°, 28° and 31.5° detected, in sample CLAP900, which effect on CLAP phase formation. Chlorapatite is still grow at 700°C for 1-hour phosphate phase at 2Θ= 25.9, 28, 31.5 and 34.

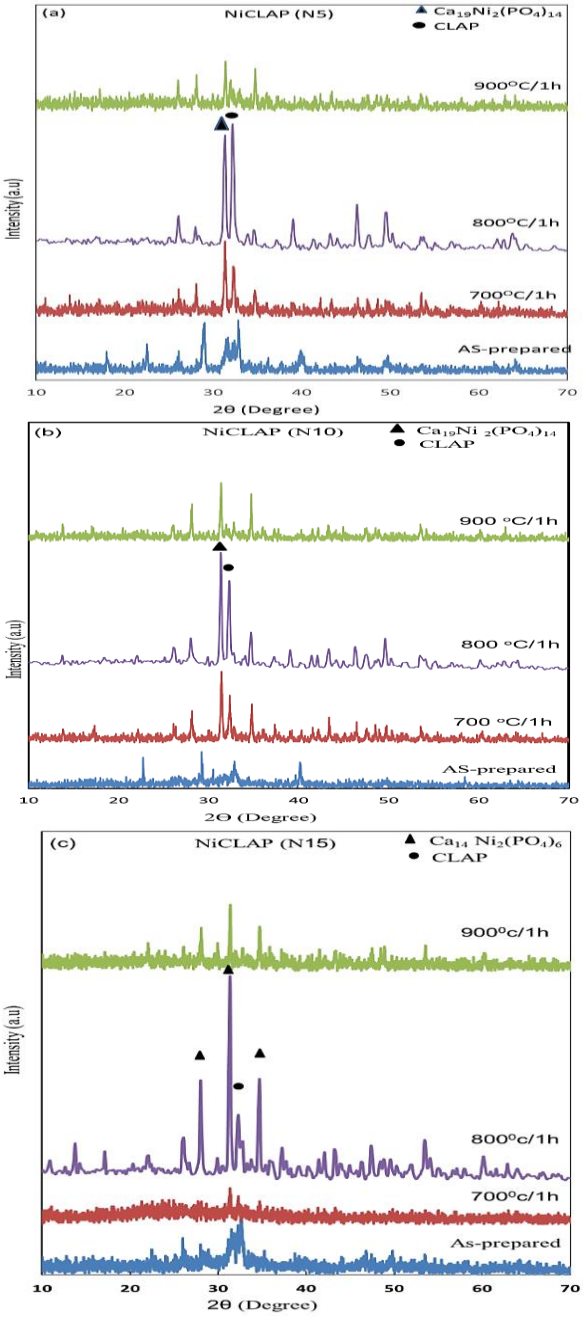

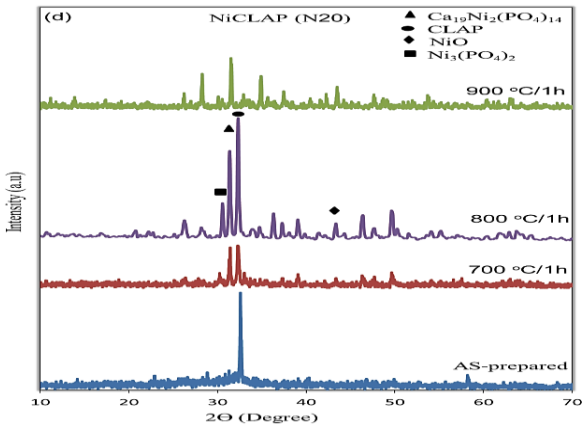

Fig. 3. (a-d) un calcined and calcined chlorapatite with different nickel concentration (5, 10, 15 and 20 mol%) at different temperatures

Table (1) shows calcium nickel phosphate% from XRD pattern, which are formed in calcined powders at different calcination temperature. It can be observing that, low calcium nickel phosphate% in calcined powder at 700 ^{o}C/1h is formed. The reason of this nature, chlorapatite sample (CLAP700) contains two phases HAP and CLAP phase, also nickel is substituted in HAP phase as well as nickel act as activating agent for forming CLAP phase.

A secondary phase (β-TCP) was detected in calcined powder at 900 ^{o}C/1h, which gives non-stoichiometric calcium nickel phosphate phase. The reason of this nature, nickel atom is doped in β-TCP phase. According to table samples at 800 ^{o}C are best substituted samples, which contain calcium nickel phosphate phase without impurities and secondary phase.

The crystalline size D of the main sharp peak for the phase of chlorapatite was calculated by using Debye Scherre equation(1) [20]

$$D = 0.91\lambda / [\beta_L \cos(\theta)], \qquad (1)$$

where λ is the copper wavelength, β_L is the integral breadths of Lorentzian part in the pseudo-Voight function of the diffraction line that has been simulated [21].

Table I Calcium nickel phosphate % at different calcite temperature

$NiCl_2$ mol%	$Ca_{19}Ni_2(PO_4)_{14}$ % 700^{0}C/1h	$Ca_{19}Ni_2(PO_4)_{14}$% 800^{0}C/1h	$Ca_{19}Ni_2(PO_4)_{14}$% 900^{0}C/1h
5	25.2	9.2	36.3
10	24.5	16.4	78.4
15	20.2	51.6	61.5
20	7.6	6.2	71.3

The CLAP700 sample presented the smallest crystallite size, approximately 35.6 nm. Linear growth was observed as a function of temperature. The crystallite size in all of the samples was less than 100 nm.as show in figure (4).

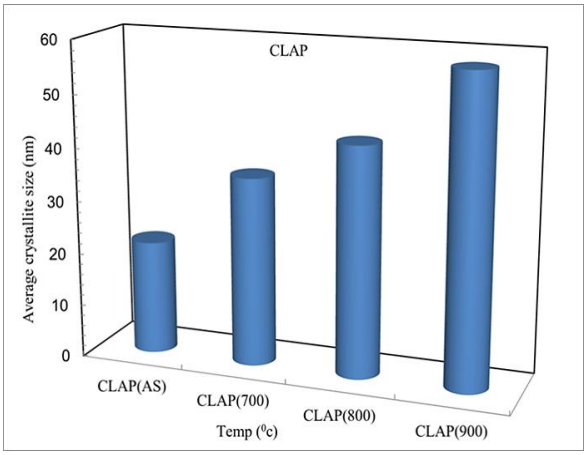

Fig. 4. Average crystallite size of as-prepared chlorapatite and chlorapatite at different calcite temperature (700°C, 800°C and 900°C).

3.2 Powder Morphology

SEM was carried out on the selected series samples were sintering at 800°C for 1 hour. All samples were coated with Au prior investigation. The stoichiometry of the samples was studied by EDX. EDX was carried out on the sample before and after sintering for 1 hour (CLAP700, CLAP800 and CLAP900), also it carried out on selected nickel doped chlorapatite sample (N15) at 800°C for 1 hour.

The morphologies of the un-calcined and calcined CLAP powders are show in figure 5 (a-d). the observed particle sizes increased slightly by increasing calcination temperature, and this correlated well with the particle size analysis results show in figure (4). A change in the surface morphology of powders was observed when the calcination temperature increased from 700 to 900°C, the phase growth from needles shape to rode shape as show in figure 5b and 5c respectively. At higher temperature, the powder particles appeared to have fused together forming larger agglomerates as show in figure 5d.

It can be concluded that the calcination has a significant effect on the particle morphology and properties. Also, it can be concluded that calcined CLAP powders at 800°C is the best heat treated for CLAP sample. By incorporation different concentration (5,10,15 and 20 mol%) of nickel particles to CLAP powders at 800°C/1h as show in figures 6 (a-d), it can be observed that sample with 15 mol %Ni doped CLAP powders at 800°C as show in figure 6-c is the more effective porous sample. It can be argued that this behavior is due to crystallinity of the synthesized powders.

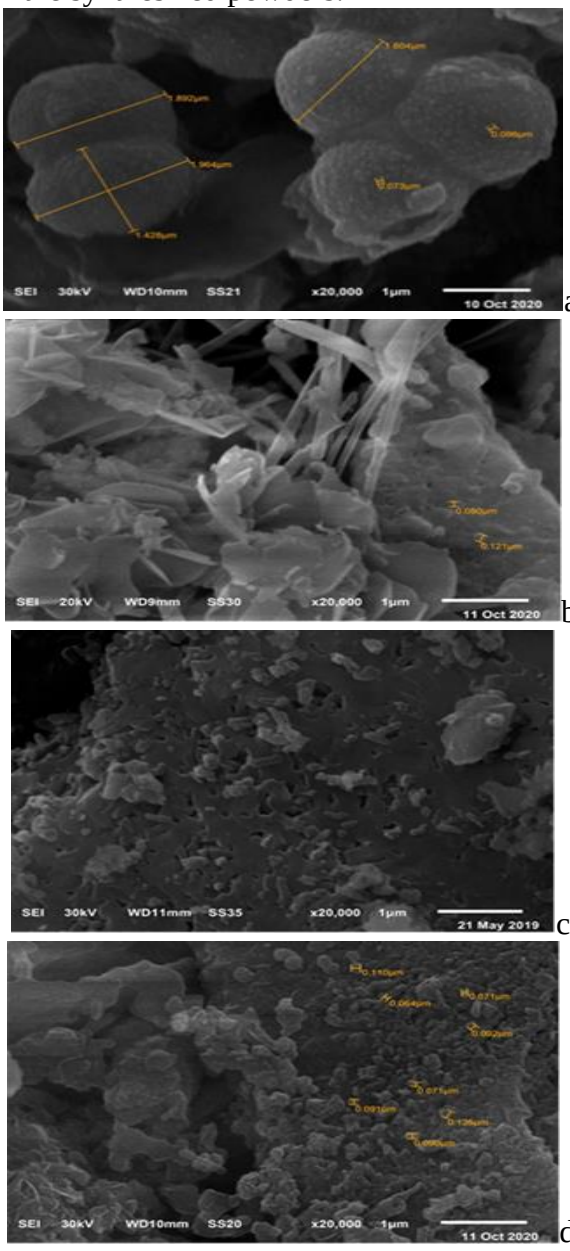

Fig. 5. (a-d) SEM images of chlorapatite at different temperature (a) as-prepared (CLAP as); (b) 700°C (CLAP700); (c) 800°C (CLAP800); and (d) 900°C (CLAP900).

3.3 Energy dispersive X-ray (EDX)

The quantitative analysis revealed that the composition ratio of calcium and phosphorous in the sample are listed in Table III as compared to the stoichiometric ratio of Ca/P (1.67) in the pure HAP powder [25]. The Ca/Cl ratio of pure CLAP, $Ca_{10}(PO_4)_6Cl_2$, is close to 5 [26]. The sample CLAP800 had the best Ca/Cl ratio,

indicating that the rise in the CLAP phase in this sample, as demonstrated by XRD and FTIR measurements.

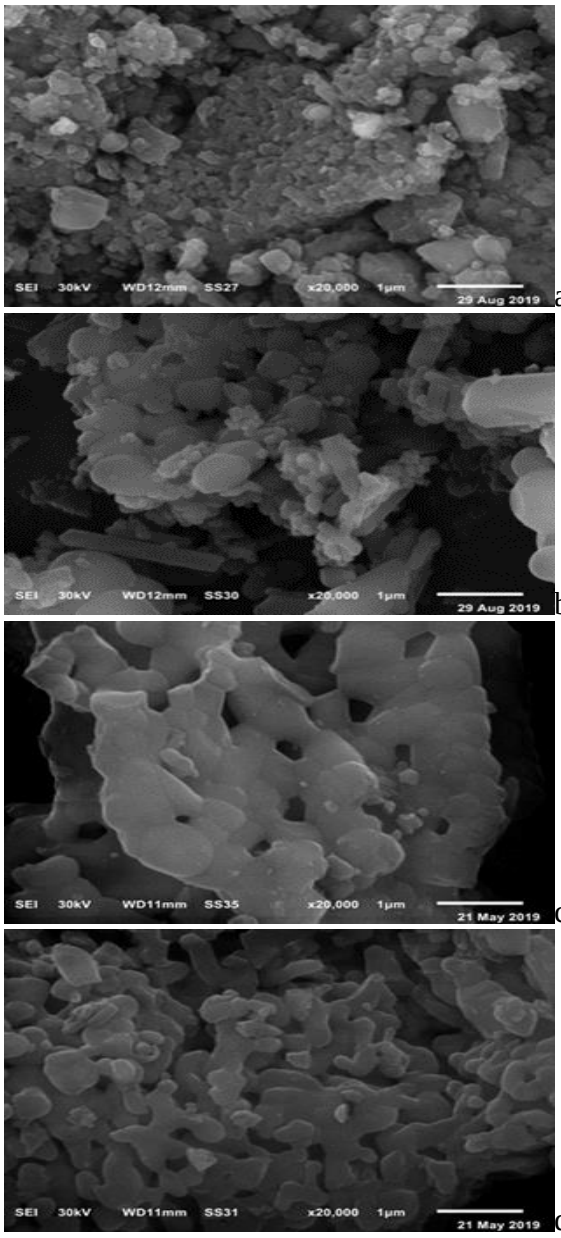

Fig. 6. (a-d) SEM images of nickel chlorapatite with different nickel concentration (5, 10,15 and 20 mol%), (a) (N5), (b) (N10), (c) (N15), and (d) (N20) at 800°C for 1 hour

Table III: EDS analysis of powder samples**.**

Atomic %						
Sample	Ca	P	O	CL	Ca/P	Ca/Cl
CLAP700	16.24	10.55	71.91	1.30	1.5	12.49
CLAP800	16	12.75	67.29	3.96	1.25	4.04
CLAP900	17.57	8.74	72.63	1.05	2.0	16.73

3.4 FTIR Spectra Analysis

The chemical stability of the samples was validated by Fourier transformed infrared spectroscopy, which also identified the functional groups present. The FTIR spectra of all CLAP powders are shown in figure (7). The spectra indicate that the broad peaks at 3400cm^{-1} (stretching) and1600 cm^{-1} (bending), which can be assigned to chemically absorbed H_2O, disappear as the calcination temperature was increased. The latter means, obtain carbonated chlorapatite in all samples treated. Carbonated chlorapatite is more stable than that of hydroxyapatite and more crystalline.

The region between 1460 and 1530 cm^{-1} is attributable to CO_3^{2-}decreased, while the band at 1382 cm^{-1} is due to the $NO_3^{2-}$and CO_3^{2-} groups vanishing as the calcination temperature is increased.

The region (560-600 cm^{-1}) and (1000-1100 cm^{-1}) are due to the PO_4^{3-} groups are still present and its height increase as the calcination temperature was increased. The persistence of the OH^- group band in as sample (N0) and disappear in calcined samples, suggests that the basic apatite structure of the samples is affected by the calcination, whereas the chemically absorbed water disappeared as the calcination temperature was increased. The band at 863 cm^{-1}is due to HPO_4^{2-} group is appearing at high calcination temperature (CLAP900), which characteristic non-stoichiometric CLAP [22].

They only contain four groups of bands due to phosphate ions that are all infrared active. In fact, the υ_3 (P-O) bands decrease of when the Nickel content increases and the υ_1 (P-O) bands appear in sample N15 and N20. The O-P-O band (υ_4) intensity increase when heat treated increase as show in figure (7), also when the Nickel content increases as show in figure 8(a-d). Those changes are probably due to a change of the PO_4 group environment caused by the Nickel introduction.

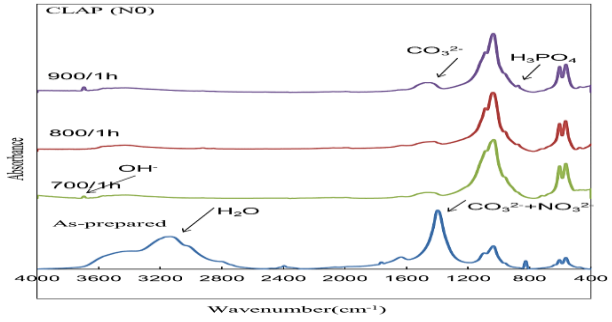

Fig. 7. FTIR spectra for un calcined and calcined chlorapatite

The observed peak at 1123 cm^{-1}, due to the presence of β-TCP [22], in sample which heat treated at 900 ^{0}C/1h, has increasing intensity by increasing Ni fraction. The occurrence of β-TCP can follow from a chemical reaction which is subjected at high temperature giving 3($Ca_3(PO_4)_2$) +CaO [23].

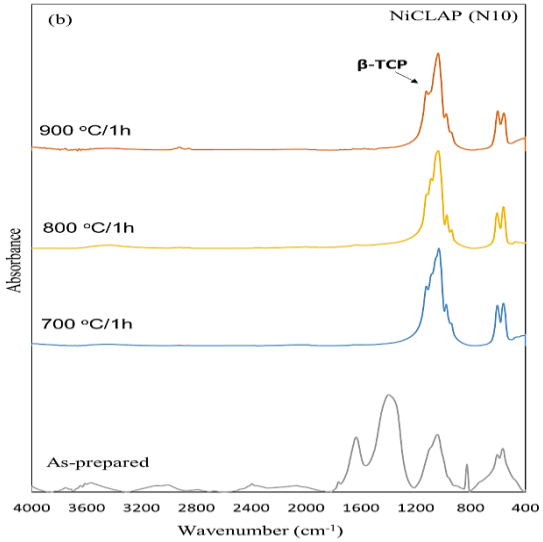

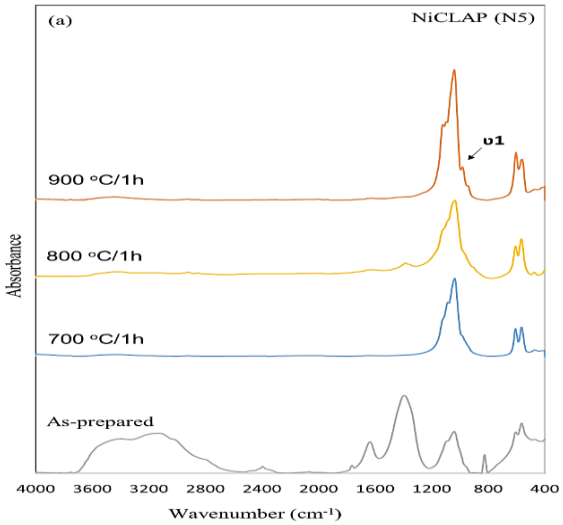

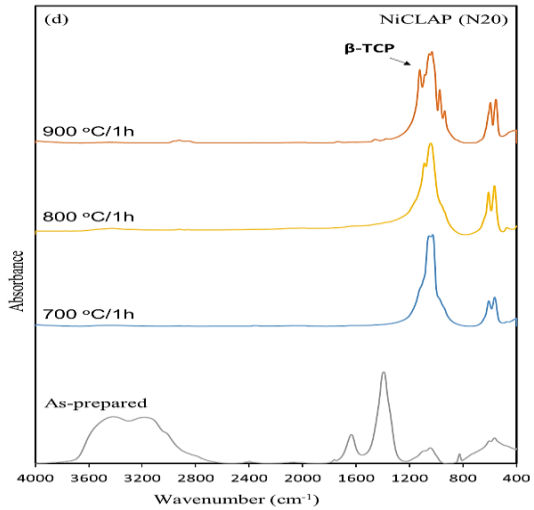

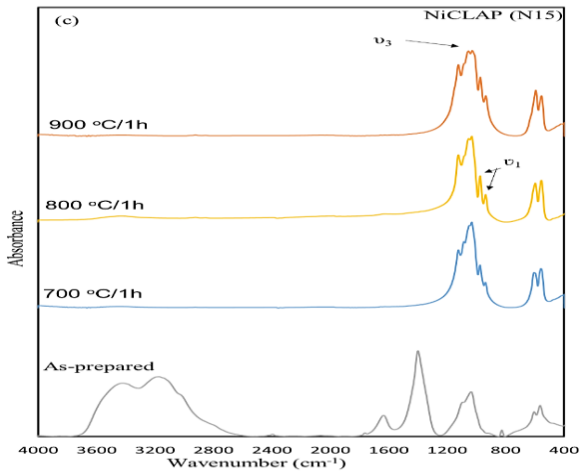

Fig. 8. (a-d) FTIR spectra for un calcined and calcined chlorapatite with different nickel concentration (5, 10, 15 and 20 mol%) at different temperature

Table II Infrared absorption bands of CLAP at700, 800, and 900°C [24]

Infrared frequency (cm^{-1})	Assignment
560 -600	PO_4 bending mode υ_4
1000-1100	PO_4 stretching mode υ_3 , υ_1
1460-1530	CO_3^{2-}
1600	OH^-
2600-3600	Adsorbed water

4. Conclusion

The main component synthesized by a solution gelation method is CLAP as the main component, calcium nickel phosphate ($Ca_{19}Ni_2(PO_4)_{14}$) as secondary component. Due to the sharpness and intensities of the spectral lines, the optimum sintering temperature is at 800°C. High percent of calcium nickel phosphate phase without impurities like $CaCl_2$ and $Ni_2P_2O_7$ formed at heat treated at 800°C for 1 hour. The average crystal size of CLAP is less than 100 nm.

The crystallite size in all of the samples was less than 100 nm. The FTIR analyses revealed the presence of Cl in the apatite channel locations and the formation of Carbonated chlorapatite, which is more stable and good crystallized than HA. The SEM confirmed that particle development was not homogeneous growth with temperature, but The CLAP800 sample has more homogeneous particles with

grains. The best Ca/Cl ratio was 4.04, which was close to the stoichiometric ratio of pure chlorapatite (CLAP). The chlorapatite (CLAP) and calcium nickel phosphate can be applied for using in west water treatment due to the fact of its adsorption capacity. Because the inclusion of some chlorine in the HA lattice can improve its resorption as well as mechanical characteristics, chlorine-substituted hydroxyapatite (HA) compound has potential in biomedical applications.

References

1 Ramadas, M., Ferreira, J. M., & Ballamurugan, A. M. (2021). Fabrication of three dimensional bioactive Sr^{2+} substituted apatite scaffolds by gel-casting technique for hard tissue regeneration, *Journal of Tissue Engineering and Regenerative Medicine*

2 Grynyuk, I. I., Vasyliuk, O. M., Prylutska, S. V., Strutynska, N. Y., Livitska, O. V., & Slobodyanik, M. S. (2021). Influence of nanoscale-modified apatite-type calcium phosphates on the biofilm formation by pathogenic microorganisms. Open Chemistry, ***19*(1),** 39-48.

3 Wołowiec, M., Tuchowska, M., Kudła, P., & Bajda, T. (2019). Synthesis and characterization of cadmium chlorapatite Cd5 $(PO_4)_3Cl$, Mineralogia, 1 (ahead-of-print)

4 Keochaiyom, B., Wan, J., Zeng, G., Huang, D., Xue, W., Hu, L., ... & Cheng, M. (2017). Synthesis and application of magnetic chlorapatite nanoparticles for zinc (II), cadmium (II) and lead (II) removal from water solutions. *Journal of colloid and interface science*, ***505*,** 824-835

5 S. Mignardi, A. Corami, V. Ferrini, (2012). Evaluation of the effectiveness of phosphatetreatment for the remediation of mine waste soils contaminated with Cd Cu, Pb, and Zn, *Chemosphere* 86, 354–360.

6 A.S. Knox, D.I. Kaplan, M.H. Paller, (2006). Phosphate sources and their suitability forremediation of contaminated soils, Sci. Total Environ. **357**, 271–279.

7 P. Miretzky, A. Fernandez-Cirelli, (2008). Phosphates for Pb immobilization in soils: areview, Environ. Chem. Lett. **6,** 121–133.

8 Li, Z., Gong, Y., Zhao, D., Dang, Z., & Lin, Z. (2021). Enhanced removal of zinc and cadmium from water using carboxymethyl cellulose-bridged chlorapatite nanoparticles, Chemosphere, **263**, 128038

9 W.N. Wang, Y. Kaihatsu, F. Iskandar, K. Okuyama, (2009). Highly luminous hollow chlorapatite phosphors formed by a template-free aerosol route for solid state lighting, Chem. Mater. **21,** 4685–4691.

10 A. Fahami, B. Nasiri-Tabrizin, R. Ebrahimi-Kahrizsangi, (2013). Mechanosynthesis and characterization of chlorapatite nanopowders, Mater. Lett. **110**, 117–121.

11 Nguyen, P. T., Nguyen, X. T., Nguyen, T. V., Nguyen, T. T., Vu, T. Q., Nguyen, H. T., ... & Thi Dinh, T. M. (2020). Treatment of Cd^{2+} and Cu^{2+} ions using modified apatite ore. *Journal of Chemistry*, *2020*

12 B. Nasiri-Tabrizi, A. Fahami,(2014). Synthesis and characterization of chlorapatite-ZnO composite nanopowders, Ceramics International, **40(2),** 2697-2706

13 T.T. Eighmy, A.E. Kinner, E.L. Shaw, J.D.E. Jr, C.A. (1999). Francis, Chlorapatite $(Ca_5(PO_4)_3Cl)$ characterization by XPS: an environmentally important secondary mineral, Surf. Sci. Spectra ***6,*** 210–218.

14 M. Srinivasan, C. Ferraris, T. White, (2006). Cadmium and lead ion capture with three dimensionally ordered macroporous hydroxyapatite, Environ. Sci. Technol. **40**, 7054–7059.

15 R. Liu, D. Zhao, (2007). Reducing leachability and bio accessibility of lead in soils using a new class of stabilized iron phosphate nanoparticles, Water Res. **41**, 2491–2502.

16 Li, Z., Gong, Y., Zhao, D., Deng, H., Dang, Z., & Lin, Z. (2021). Field assessment of carboxymethyl cellulose bridged chlorapatite microparticles for immobilization of lead in soil: Effectiveness, long-term stability, and mechanism. Science of The Total Environment, 146757.

17 ARGUETA-FIGUEROA, Liliana, et al. Synthesis, characterization and antibacterial activity of copper, nickel and bimetallic Cu–Ni nanoparticles for potential use in dental materials. Progress in Natural

Science: Materials International, 2014, 24.4: 321-328.
18 Anand, G. T., Nithiyavathi, R., Ramesh, R., Sundaram, S. J., & Kaviyarasu, K. (2020). Structural and optical properties of nickel oxide nanoparticles: Investigation of antimicrobial applications. Surfaces and Interfaces, **18,** 100460
19 Yadav, S., Ali, A., Krishnamurthy, S., Singh, P., & Pyare, R. (2021). In-vitro analysis of bioactivity, hemolysis, and mechanical properties of Zn substituted Calcium Zirconium silicate (baghdadite). Ceramics International, **47(11)**, 1, 16037-16053
20 Cullity, B.D (1956). Elements of X-ray Diffraction; Addison-Wesley Publishing: Massachusetts, United States of America,;
21 Takeno, M.L.; da Silva, G.A.; Trichês, D.M.; Ghosh, A.; de Souza, S.M. (2018) Structural studies of the layered SnSe produced by mechanical alloying and melting technique. *J. Alloy. Compd*., **735**, 489–495.
22 El Feki, H., et al., (2004) Synthesis of potassium chloroapatites, IR, X-ray and Raman studies. physica status solidi (c) 1.7: 1985-1988.
23 Piga, G., Amarante, A., Makhoul, C., Cunha, E., Malgosa, A., Enzo, S., & Gonçalves, D. (2018). β-Tricalcium phosphate interferes with the assessment of crystallinity in burned skeletal remains. *Journal of Spectroscopy*, ID 5954146 | https://doi.org/10.1155/2018/5954146.
24 Campos, P. V., Albuquerque, A. R. L., Angélica, R. S., & Paz, S.P.A. (2021). FTIR spectral signatures of amazon inorganic phosphates: Igneous, weathering, and biogenetic origin. Spectrochimica Acta Part A: Molecular and Biomolecular Spectroscopy, **251**, 119476.
25 Labjar, H., & Chaair, H. (2021). Synthesis and characterization of apatite silicated powders with wet precipitation method. In E3S Web of Conferences (Vol. **234**, p. 00106). EDP Sciences
26 Cavalcante, L. D. A., Ribeiro, L. S., Takeno, M. L., Aum, P. T. P., Aum, Y. K. P. G., & Andrade, J. C. S. (2020). Chlorapatite Derived from Fish Scales. Materials**,** ***13*****(5),** 1129